atmosphere

MDPI

Article

^{210}Pb Deposition Distribution in the Northern Hemisphere Based on a Long-Range Atmospheric Transport and Deposition Model Calculation

Yu Cai [1,*], Hiromi Yamazawa [2] and Takeshi Iimoto [1]

[1] Department of Environmental Systems, Graduate School of Frontier Sciences, The University of Tokyo, Tokyo 227-8568, Japan; iimototakeshi@g.ecc.u-tokyo.ac.jp
[2] Department of Applied Energy, Graduate School of Engineering, Nagoya University, Nagoya 464-8603, Japan; yamazawa@energy.nagoya-u.ac.jp
* Correspondence: 6056643479@edu.k.u-tokyo.ac.jp

Abstract: This study delves into the long-term atmospheric transport and deposition of ^{210}Pb in the Northern Hemisphere by using the atmospheric transport model HIRAT. The calculation for the four-year (2012–2015) period showed an average deposition flux of 13.0 Bq m^{-2} month^{-1} with significant seasonal variations characterized by higher deposition rates during summer and lower during winter. High deposition was found in the Northern Bay of Bengal and Bangladesh regions, Southern China, the Western Philippine Sea, the Eastern Japan Sea, the Northwestern Pacific region, the Eastern and Western coasts of North America, the Caribbean Sea, the Eastern Pacific region off of Central America, the Central Atlantic region between Central America and Africa, and the Northwestern Atlantic Ocean. Deposition patterns varied across latitudinal zones, with tropical areas experiencing the highest deposition and polar/subpolar zones the lowest. This study emphasized the impact of monsoons on the significantly large ^{210}Pb deposition in the Japan Sea region. Furthermore, this study showed that the lower troposphere (0 to 3 km) dominates with about 53%, and the middle troposphere (3 to 6 km) and upper troposphere (above 6 km) also contribute significantly to the total ^{210}Pb inventory with 37% and 10%, respectively. These findings provide essential insights into the characteristics of atmospheric transport and deposition of ^{210}Pb, and their mechanisms.

Keywords: ^{210}Pb deposition; ^{222}Rn; atmospheric transport model; environmental radioactivity

Citation: Cai, Y.; Yamazawa, H.; Iimoto, T. ^{210}Pb Deposition Distribution in the Northern Hemisphere Based on a Long-Range Atmospheric Transport and Deposition Model Calculation. *Atmosphere* **2023**, *14*, 1329. https://doi.org/10.3390/atmos14091329

Academic Editor: Giacomo Alessandro Gerosa

Received: 31 July 2023
Revised: 21 August 2023
Accepted: 21 August 2023
Published: 23 August 2023

1. Introduction

The worldwide average dose of 2.4 mSv y^{-1} from natural sources has been reported by the United Nations in the United Nations Scientific Committee on the Effects of Atomic Radiation (UNSCEAR) 2008 Report [1]. In another report, the dose for Japanese was reported to be 2.1 mSv y^{-1}, which is just slightly less than the world average [2]. However, it is of interest that the dose of 0.99 mSv y^{-1} is from food ingestion because it is nearly three times the world average. It is well known that seafood accounts for a large proportion of the daily diet of Japanese people, and very high depositions of ^{210}Pb were observed along the Japan Sea coastline in winter, and they were considered to be caused by atmospheric transport of these radon decay nuclides from the Asian continent by the winter monsoon in the East Asia region [3,4]. Therefore, it can be supposed that the deposited ^{210}Pb and ^{210}Po that are transferred to seafood and ingested orally are the main sources of the internal dose to the Japanese population, although this hypothesis has not been proved. Therefore, the analysis of the distribution and behavior of ^{222}Rn and its decay nuclides in the atmosphere over the globe can provide a deeper and broader understanding of the radiation dose due to oral ingestion.

^{210}Pb (half-life 22.3 year) and its progeny ^{210}Po (half-life 138 day) are nuclides in the decay chain of ^{222}Rn (half-life 3.82 day) exhaled from soil surfaces and transported

through the atmosphere, and they are deposited on land and ocean surfaces mainly by precipitation. Atmospheric ^{222}Rn and its daughter nuclides ^{210}Pb have also been widely used as efficient atmospheric tracers to quantify atmospheric transport processes [5]. Alonso-Hernández et al. [6] provided data on the ^{210}Pb monthly deposition flux, which varied between 1.24 and 8.29 Bq m^{-2} month^{-1} with an average of 3.97 Bq m^{-2} month^{-1} at Cienfuegos, Cuba, for 11 months, from 2010 to 2011. Magnoni et al. [7] reported a monthly deposition of 19.3 Bq m^{-2} month^{-1} in Italy during 2005–2021. Leppänen et al. [8] provided data observed at Sodankylä and Rovaniemi in Finland in 2014, where the annual deposition flux was 66 and 55 Bq m^{-2} y^{-1}, respectively. Peng et al. [9] provide deposition flux data from two Chinese sites in 2012 and 2016 of 0.45 and 0.41 Bq m^{-2} d^{-1} at Yueyang and 0.76 and 0.93 Bq m^{-2} d^{-1} at Hengyang. According to Lozano et al. [10] and references therein, deposition fluxes of 34–121 Bq m^{-2} y^{-1} measured at different locations in Spain, Italy and France were reported. In contrast to these relatively small values, Yamamoto et al. [4] confirmed an anomalously high deposition of ^{210}Pb on the Sea of Japan coastline of the main island of Japan, with the maximum annual deposition flux exceeding 1000 Bq m^{-2} y^{-1}. Hirose et al. [3] reported deposition fluxes at sites in Japan in 2000, which ranged from 465 to 800 Bq m^{-2} y^{-1} along the Japan Sea coastline and 97–322 Bq m^{-2} y^{-1} at other locations in Japan. These observations all reported that precipitation played a very important role [11]. However, the very limited number of measurement sites reporting ^{210}Pb deposition makes it difficult to depict the spatial distribution of deposition in detail. The observation point can only observe localized deposition values and cannot necessarily represent the amount of deposition in an area with a certain horizontal extent due to its high dependence on the geographic location [12,13]. It is also difficult to understand the processes of atmospheric transport and the deposition of ^{210}Pb when determining the spatial and temporal variability in deposition flux only from these observations.

In our previous research, we developed a long-range atmospheric transport/deposition model for ^{222}Rn and its progenies [14]. Based on our preliminary calculations with a horizontal resolution of 9 km around the Japanese mainland and the Sea of Japan [13], the model successfully reproduces a substantial amount of ^{210}Pb depositions along the coastline of the Sea of Japan, reaching up to approximately 200 Bq m^{-2} month^{-1}, which is about ten times higher than the deposition on the Pacific Ocean side of Japan during winter [15]. The simulation also successfully reproduced features in the observed deposition distribution in which a heavier deposition was observed in the central part of the Sea of Japan coastline in winter than in the western part of it [3]. However, deposition and precipitation at Rokkasho in the Aomori prefecture in Japan in winter were significantly underestimated. Subsequently, we implemented a finer horizontal resolution of a 3 km grid to enhance the model's reproducibility. The results demonstrated a considerable improvement in reproducing the values at Rokkasho compared to the observed value of 189 Bq m^{-2} month^{-1} in December 2015. Although the model has not been fully validated for the deposition caused by small-scale precipitation under the influence of local terrain, the model successfully reproduced the ^{210}Pb deposition caused by monsoon-scale meteorological conditions [12].

The purpose of this study is to characterize the distribution and seasonal variations of ^{210}Pb deposition in the Northern Hemisphere. In addition to the general features in deposition patterns in the Northern Hemisphere, such as the latitudinal distribution, characteristics in the Far East area are of specific interest to this study. Through the analysis of spatial and temporal patterns of atmospheric concentration and the deposition of ^{210}Pb, we aim to gain insights into the general mechanisms driving their variability in transport and deposition across different regions and seasons.

2. Materials and Methods

The deposition flux distribution of ^{210}Pb in the Northern Hemisphere was analyzed by carrying out long-term simulations of atmospheric transport and the deposition of ^{222}Rn and its decay products from ^{218}Po to ^{210}Pb. The model used comprises two components: the meteorological model, WRF (weather research and forecasting model) Ver.4 [16], and

the long-range transport model, HIRAT [14]. This combination of models has been successfully validated and applied to analyze the ^{210}Pb deposition in Japan [12,13]. A detailed description of the model can be found in our previous reports, and only the outline of the model is described as follows.

2.1. Meteorological Model

The framework of the WRF is a three-dimensional, non-hydrostatic, fully compressible Navier–Stokes equation system. The WRF computes three-dimensional fields of wind speed, vertical dispersion coefficients and atmospheric cloud water/ice content, as well as two-dimensional precipitation fields (rain and snow) using input data of coarse-gridded meteorological data from meteorological agencies. This model has long been widely used as a community model in the meteorological and atmospheric environmental fields. The physical options in the WRF calculation used in this study are as follows.

The cloud microphysics model, WSM (WRF single-moment 5-class), quantifies the water–mass mixing ratio of water vapor, rain, snow, cloud water and cloud ice [17]. The longwave radiation model, RRTM (rapid radiative transfer model), calculates longwave (infrared) radiation transfer by incorporating various forms of gases and particles that affect the radiation transfer in the atmosphere [18]. The Dudhia scheme was used to accommodate cloud absorption and the scattering of shortwave (visible) radiation [18]. The Noah land surface model [18] was used to characterize four layers of soil temperature, moisture, snow cover, and frozen soil. The boundary layer turbulence was represented by the MYNN (Mellor–Yamada–Nakanishi–Niino) closure model [19] to calculate the vertical turbulence diffusivity that governs the vertical diffusion of ^{222}Rn and its progenies. The Kain–Fritsch scheme was used to evaluate sub-grid scale cumulus precipitation. The output from this scheme, together with the output WSM form, constitutes precipitation on the Earth's surface that is used to describe a wet deposition.

2.2. Advection–Diffusion Model

The advection–diffusion equation used in the HIRAT for the concentration Q of a nuclide is expressed as follows. The left-hand side is a temporal change in the atmospheric concentration. The first three terms on the right-hand side are the advection terms, the fourth term is the vertical diffusion term, and the last term is the source/sink term. See Appendix A Table A1 for other variables.

$$\frac{\partial hQ}{\partial t} = -m^2 \frac{\partial}{\partial x}\left(\frac{huQ}{m}\right) - m^2 \frac{\partial}{\partial y}\left(\frac{hvQ}{m}\right) - \frac{\partial hw^*Q}{\partial z^*} + \left(\frac{z_t}{h}\right)^2 \frac{\partial}{\partial z^*}\left(hK_{z^*}\frac{\partial Q}{\partial z^*}\right) + hS \quad (1)$$

where the horizontal coordinates are x and y, and the terrain following the z^* coordinate system is for the vertical:

$$z^* = \frac{z_t(z - z_g)}{h},\ h = z_t - z_g \quad (2)$$

where w^* is the vertical wind speed in the z^* coordinate; the turbulent diffusion accounts only for the vertical direction because horizontal diffusion does not play a significant role in the hemispheric scale as compared with the horizontal advection. The map factor m accounts for the distortion of length due to the map projection used to convert the curvature of the Earth's surface to the flat x-y plane. The sink/source term S represents not only the dry and wet deposition processes but also the gain from the parent nuclide's decay and loss of the nuclide of interest by its decay to progeny, as described in the next section.

The location of the grid points is based on the Arakawa-C grid [20]. All scalar quantities are in the center of the grid. The momentum component is the average of each surface; however, the scalar quantity (mass/thermodynamic/chemistry quantities) is the average value of the entire grid cell. The velocities u and v in the x and y directions are arranged at the same positions as the scalar in the vertical direction and semi-grid offset from the center of the grid in the horizontal direction perpendicular to each surface. The velocity w^*

in the z direction is arranged at the same position as the scalar in the horizontal direction and semi-grid offset in the vertical direction.

In solving this Equation (1), the HIRAT uses the HIFI method [21] for the finite difference representation of the advection terms, which uses a combination of the first-order finite difference method, the second-order finite difference method, and the FI method depending on the gradient of concentration. This makes it possible to reduce the pseudo-diffusion while suppressing the calculation cost. For the diffusion term, the Crank–Nicolson method with second-order accuracy was used [22].

2.3. Source/Sink Term

The source/sink term can be expressed as follows:

$$S = S_{source} + S_{dry} + S_{wet} + S_{decay} \tag{3}$$

S_{source} is the source term described below; S_{dry} *is* the dry deposition term; S_{wet} *is* the wet deposition term; and S_{decay} *is* the decay term. For the N-th nuclide that has decayed from its parent, the source term is expressed in the following equation when Q is the number of atoms in the unit volume of the atmosphere:

$$S_{source_N} = \lambda_{N-1} \cdot Q_{N-1} \tag{4}$$

This source term does not appear in the equation for ^{222}Rn because it has no volume source. The source of ^{222}Rn is expressed as a bottom boundary condition, as described in Section 2.4.

The decay term is expressed as follows:

$$S_{decay_N} = -\lambda_N \cdot Q_N \tag{5}$$

where λ_N is the decay constant of the N-th nuclide.

It is assumed that nuclides decaying from ^{222}Rn are removed from the atmosphere by dry and wet depositions and brought to the Earth's surface as fallout, whereas ^{222}Rn is free from these deposition processes. A dry deposition was applied to the bottom atmospheric layer of the model by simply expressing it in terms of the constant deposition velocity v_d (=1.0×10^{-3} m s^{-1}) regardless of the type of ground surface and meteorological conditions. The simplicity of this approach can be justified due to the fact that the dry deposition does not so significantly affect the results as compared with a wet deposition in determining the overall total deposition.

$$S_{dry_N} = -v_d \cdot (Q_N)_1 \cdot \frac{1}{\delta z_1} \tag{6}$$

where $(Q_N)_1$ is the concentration of the N-th nuclide in the first (bottom) atmospheric layer of the model, whose depth is δz_1.

Wet deposition is a phenomenon in which liquid or solid water in the atmosphere takes in and carries the nuclides to the ground's surface. There are two types of wet deposition processes. Washout is the process in which nuclides are taken up in rain or snow during their descent under clouds, whereas rainout is the process in which the nuclides are taken up by hydrometers during rain formation in clouds. Since both processes depend on many parameters, such as the size distributions of cloud droplets and raindrops, aerosol size distribution, and precipitation intensity, it is difficult to reproduce the actual situation, and thus, in this study, a commonly used empirical formulation was adopted. The wet deposition can be expressed by the following equation:

$$S_{wet_N} = -\Lambda \cdot Q_N \tag{7}$$

The scavenging coefficient Λ defined by the following equation was used.

$$\Lambda = \alpha\ I^{\beta} \tag{8}$$

where α and β are empirical constants and I is the precipitation intensity in mm h^{-1}. Considering rain and snow separately, the parameters used were $\alpha = 8.0 \times 10^{-5}$ s^{-1} and $\beta = 0.8$ for rain, and $\alpha = 8.0 \times 10^{-5}$ s^{-1} and $\beta = 0.3$ for snow [19].

Since the output time interval of WRF is 3 h, the amount of precipitation in HIRAT was set to a constant value for 3 h. The wet deposition was applied only to the atmospheric layers within and under clouds. The presence of clouds was determined using a cloud–water (plus ice) mixing ratio q_c larger than 1.0×10^{-6}.

2.4. Simulation Conditions

The following input data were used: the Japan Meteorological Agency's 6-hourly global meteorological analysis data (JMA GANAL) for the three-dimensional meteorological field, JMA's sea daily sea surface temperature (JMA-MGDSST), soil data from the National Center for Environmental Prediction's Final Operational Analysis data (NCEP-FNL), and land use data from the US Geological Survey (USGS). They were used to initialize the meteorological calculations and to nudge the calculations by using a data assimilation function of WRF.

The source of ^{222}Rn was given as flux from the ground surface through the bottom boundary condition of the first layer of the atmosphere. The initial radon concentration in the atmosphere was assumed to be zero, and a spin-up calculation period of 15 days was set to build up the atmospheric concentration field at the beginning of the period of interest. This study used a combination of two global ^{222}Rn flux maps to represent the surface flux patterns of ^{222}Rn in the Northern Hemisphere. Schery's map [23] provides reasonable estimations of ^{222}Rn flux below the 50°N latitude but tends to exhibit an overestimation in high-latitude regions [24]. The same paper pointed out that Hirao's map [25] yielded better estimates of ^{222}Rn fluxes in the middle and high latitudes, particularly across the Siberian region, than Schery's map. Both flux maps are based on a similar principle in which diffusion of ^{222}Rn in the surface soil layer is expressed by a one-dimensional diffusion equation, and the emanation power and the diffusion coefficient of ^{222}Rn are parameterized as functions of the ^{226}Ra content in soil, soil moisture and temperature. The two flux maps use similar but different sets of parameterizations and input data of ^{226}Ra content, soil moisture and temperature. The ^{222}Rn flux is given at each $1^{\circ} \times 1^{\circ}$ grid cell of the globe.

In the present study, Schery's map was used for the regions below 40° N, while Hirao's map was applied for the regions above 60° N. In the intermediate zone between 40° N and 60° N, a hybrid map was employed, giving Hirao's map a weight of (latitude-−40)/20. This comprehensive approach effectively suppresses excessive flux at high latitudes while maintaining the superiority of Schery's map for reproducibility in mid-latitudes and lower latitudes. Because both maps had been given for each month, the present calculation used monthly maps in which the ^{222}Rn flux was constant during the month. The annual average horizontal distribution of the radon flux used in the present study is shown in Figure 1. The ^{222}Rn flux over the ocean was set at a constant value of 0.14 Bq m^{-2} s^{-1}.

The meteorological and transport/deposition calculations were conducted using a horizontal grid interval of 144 km × 144 km. The calculation domain was represented by 170 × 170 grids, which encompassed the entire Northern Hemisphere with a polar stereographic projection with the North Pole at the center. The vertical discretization comprised 34 layers, extending from the surface up to an altitude of 10 km. The vertical grid spacing was variable, with the lowest layer having a depth of 10 m and gradually increasing with height. Above 5000 m from sea level, a fixed grid spacing of 1000 m was implemented. The calculations were performed with a time step of 180 s, and the resulting precipitation, deposition and concentration data were stored on an hourly basis. Additionally, the calculation period spanned a four-year interval from the beginning of

2012 to the end of 2015. Each year's calculations were executed independently, preceded by a meticulously designed 15-day spin-up period.

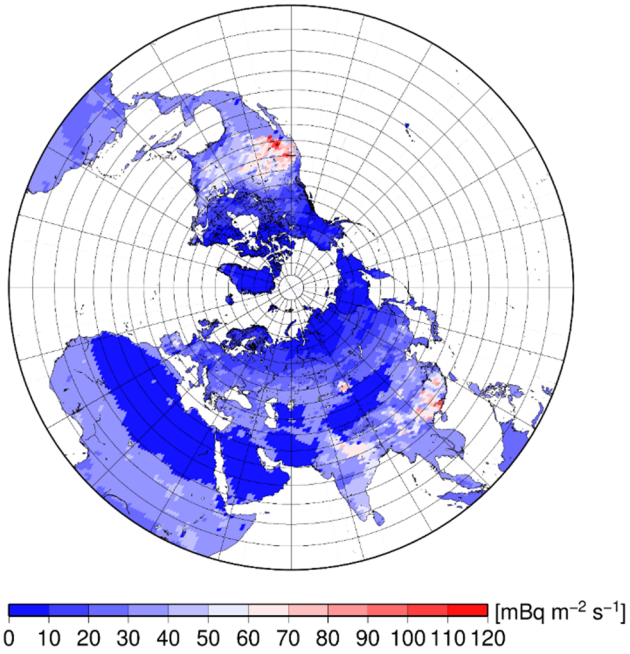

Figure 1. Annual average ^{222}Rn flux from the ground surface.

3. Results

3.1. Deposition Distribution of ^{210}Pb

Figure 2 illustrates the ^{210}Pb deposition and average residence time calculated for the period 20122015. The calculation method and description of the average residence time are detailed in Section 3.2. The ^{210}Pb deposition in Figure 2 shows that the highest monthly deposition in the Northern Hemisphere occurred in August with 16.6 Bq m^{-2} month^{-1}, and the lowest deposition occurred in February with 10.0 Bq m^{-2} month^{-1}. The average deposition flux in summer and autumn is significantly higher than in spring and winter, and the four-year average deposition flux was 13.0 Bq m^{-2} month^{-1}, with a difference between years being less than 0.8 Bq m^{-2} month^{-1}. As discussed below, the average deposition flux varies spatially from less than 10 Bq m^{-2} month^{-1} to more than 60 Bq m^{-2} month^{-1}.

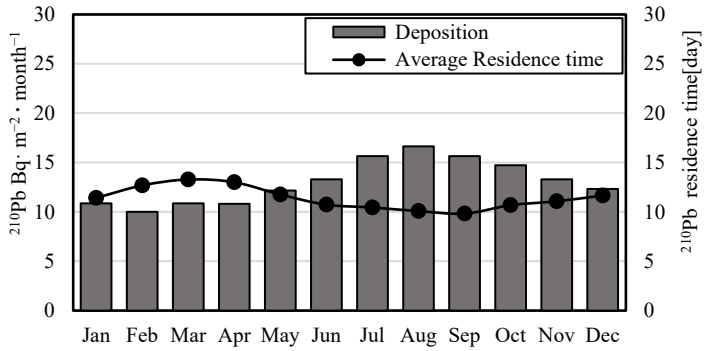

Figure 2. Monthly average of deposition flux and residence time composited over the four years from 2012 to 2015.

The distribution of high deposition in the Northern Hemisphere is characterized by distinct geographical features, as shown in Figure 3. Significant high deposition distributions (i.e., about twice the world average) are found in the Northern Bay of Bengal and Bangladesh region, Southern China, the Western Philippine Sea, the Eastern Japan Sea,

the Northwestern Pacific region, the Eastern and Western coasts of Canada and North America, the Caribbean Sea, the Eastern Pacific region off Central America, the Central Atlantic region between Central America and Africa, and the Northwestern Atlantic Ocean. Some of these regions reach about three times the world average, e.g., the Sea of Japan and the North Atlantic Ocean. Some of them reach 4–5 times the world average, e.g., the Central American region, although the deposition fluxes are considered to be smoothed by the large horizontal grid cell of 144 × 144 km^2 in which local flux maxima, if any, are not explicitly represented by the calculation.

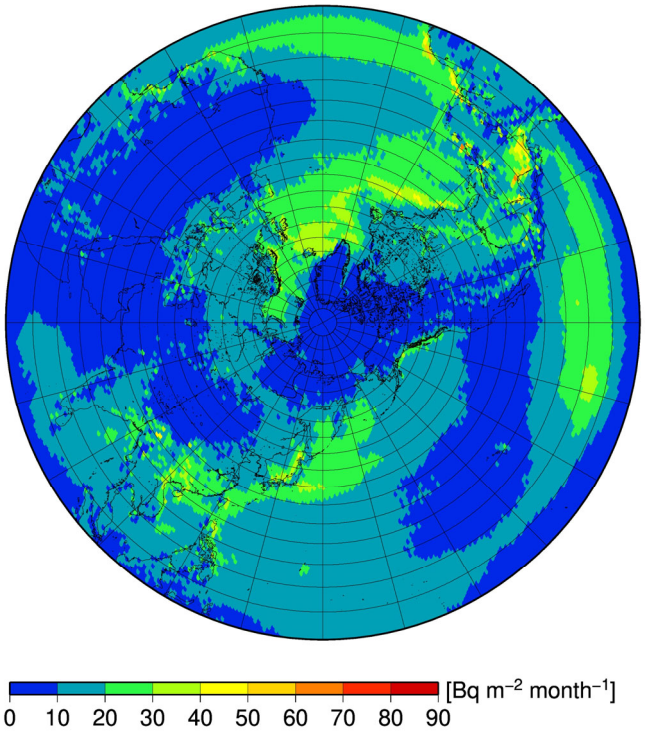

Figure 3. Distribution of annual ^{210}Pb deposition averaged for the four years from 2012 to 2015.

The regional distribution of low deposition is concentrated in the Arctic, Northern Africa, the Arabian region, Northwestern China to the Himalayas, the western part of North America, and the Eastern Pacific Ocean. The distribution of deposition seems to be strongly correlated with the distribution of monsoons. Most of the high deposition regions are found at the downwind areas of monsoons from continental regions. High deposition was found near mountain ranges, such as those in Bengal and Northeast India, in Japan, and near the Rocky Mountains in North America.

3.2. ^{210}Pb Residence Time in the Atmosphere

In this study, the residence time of ^{210}Pb in the atmosphere was also taken into consideration. The residence time τ [d] can be expressed as the following equation:

$$\tau = C/D \tag{9}$$

where C [Bq m^{-2}] is the ^{210}Pb concentration in an air column, which was calculated by integrating the atmospheric ^{210}Pb in the vertical direction from the bottom to the top of the model domain; D [Bq m^{-2} d^{-1}] is the calculated deposition flux. This computation is performed for each grid in the calculation domain.

The monthly average residence time is shown in Figure 2. The average for the whole domain and calculation period evaluated is 12.1 days. The difference between the four annual averages is shorter than 1 day. The trend in residence time is basically in the opposite sense of the deposition trend. The residence times in winter and spring are longer than

that in summer and autumn, with the longest being 13.3 days in March and the shortest being 9.9 days in September. The month with the longest residence time was delayed behind the month of the lowest deposition by one month. The hemispheric distribution of the residence time is shown in Figure 4. There are regions where the average residence time is more than 30 days, e.g., the Arctic, Central Asia, the Arabian Peninsula and the Sahara Desert, whereas there are regions where the average residence time is shorter than average, around 3–10 days (light blue portion on the scale). In some areas with very high depositions, such as the Philippine Sea or the Caribbean Sea, the average residence time can be as short as less than 3 days (Figure 4).

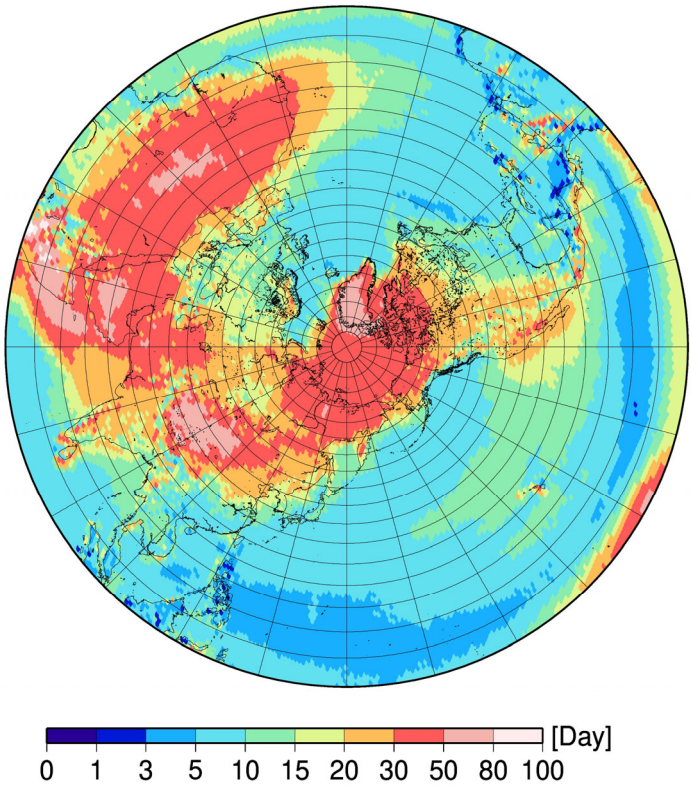

Figure 4. ^{210}Pb residence time averaged for the four years from 2012 to 2015.

3.3. Comparison with Observation

The reproducibility of the model was verified in the Japanese region in our previous study [13], in which the observed clear contrast in ^{210}Pb deposition flux—with deposition one order of magnitude higher on the Sea of Japan side of the Main Island of Japan than that on the Pacific side—was successfully reproduced by the model. To clarify the reproducibility of the results of this calculation in the Northern Hemisphere region, the present calculation results were compared with the observational results reported in the literature.

The observed monthly ^{210}Pb deposition at Yueyang (29°21′ N, 113°00′ E) and Hengyang (26°45′ N, 112°34′ E) in China in 2012, calculated by the model, were compared with the observation by Peng et al. [9] in Figure 5. The calculation is close to the observation at Yueyang, and the seasonal variations are similar, although the deposition in the last half of the observation period is overestimated. Whereas the observed deposition in winter at Hengyang is well reproduced, and the calculated values in summer are underestimated.

The observed annual deposition flux of 140 Bq m^{-2} y^{-1} at Xiamen (24°26′ N, 118°06′ E) in 2011 [26] was reasonably reproduced by the present calculation as the four-year average annual deposition flux of 121.5 Bq m^{-2} y^{-1}. The calculated annual depositional flux of 150 Bq m^{-2} y^{-1} is overestimated compared to the reported annual ^{210}Pb deposition flux of 34 Bq m^{-2} y^{-1} in Italy and Spain in the Mediterranean region [10]. However, the calculated annual depositional flux of 161 Bq m^{-2} y^{-1} is close to the reported annual

flux of 121 Bq m^{-2} y^{-1} at the observation site in France. The annual deposition flux observed at Neuherberg (43°08′ N, 11°35′ E) is 180 Bq m^{-2} y^{-1} [27], and the calculated annual depositional flux of 182 Bq m^{-2} y^{-1} is in good agreement with the observed value. The aerosol residence time in the atmosphere in 1996 was observed in two sites [11]: in Poker flat (65°06′ N, 147°30′ W), Alaska, it was reported to be 32 days in January, and the present calculation resulted in 44 days; at Eagle (65°54′ N, 141°12′ W), the residence times of 9.5–38.7 days were observed in March, and the corresponding calculation results in this study was 38 days. The mean residence times at these two locations were reasonably estimated. Ali et al. measured an annual deposition flux of 1–129 Bq m^{-2} y^{-1} at Murree (33° 53′ N, 73° 41′ E) in Pakistan and 1137 Bq m^{-2} y^{-1} at Islamabad (33° 38′ N, 73° 09′ E) [28]. These two sites are in the same grid in our model, and their annual deposition fluxes were 190 Bq m^{-2} y^{-1} in the calculations of this study. The size of the horizontal grid in the present calculation was highly probable to be too coarse to resolve the localized and very high deposition at Murree.

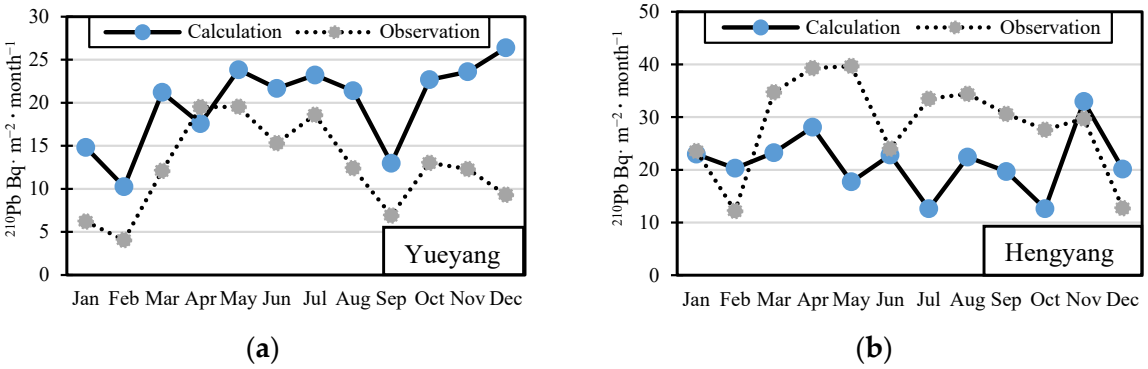

Figure 5. Comparison of calculated monthly deposition fluxes of ^{210}Pb with observed values in 2012: (**a**) Yue yang; (**b**) Hengyang [9].

In summary, to verify the reproducibility of the calculations in the Northern Hemisphere, several observations from China, Europe, Alaska and Pakistan with different climatic and geographic characteristics were compared. The calculations in this study reproduce deposition in the Northern Hemisphere generally well.

4. Discussion

4.1. Latitudinal Variation

The spatial distribution shown in Figure 3 clearly illustrates the dependence of deposition patterns on climate and ocean–land distribution. To illustrate the former, the Northern Hemisphere is divided into four latitudinal zones for analysis based on the different climatic environments of the different latitudinal zones. The tropical zone in the region of 0–15° N primarily corresponds to the intertropical convergence zone (ITCZ) activity in the Northern Hemisphere, where a seasonal change in climate is inconspicuous, with constant year-round high temperatures and abundant precipitation. The subtropical zone of 15–30° N is intended for seeing characteristics in the semi-arid and semi-humid zones, and it is strongly influenced by the ITCZ with strong seasonal changes. The mid-latitude zone at 30–60° N generally has four distinct seasons, with variable climate patterns and large seasonal temperature and precipitation variations. The polar/subpolar zones of 60–90° N has very low precipitation.

The annual averages of deposition flux and residence time of ^{210}Pb are shown in Table 1. Higher average deposition fluxes are found in the tropical zone (14.0 Bq m^{-2} $month^{-1}$) and the mid-latitude zone (14.8 Bq m^{-2} $month^{-1}$), where precipitation is abundant. In contrast, deposition was lower in the polar/subpolar zones (11.3 Bq m^{-2} $month^{-1}$) and the subtropical zone (12.0 Bq m^{-2} $month^{-1}$). A large portion of the deposition in the mid-latitude zone is distributed in the oceanic region (Figure 3). Additionally, according to Figure 4, the atmospheric residence time of ^{210}Pb is longer at the polar/subpolar zones

(19.7 day), which is nearly three times that of the equatorial region. In this latitude zone, the residence time is long in the continental part, reaching more than 30 days, and in the North Atlantic, it is as short as around 5 days. This is consistent with the observed characterization of the global atmospheric deposition flux of ^{210} Pb, which is higher in the tropics and mid-latitudes and lowest in the polar regions [5].

Table 1. Annual averages of deposition flux and residence time across latitude zones.

Latitude Zone	^{210}Pb Deposition Flux (Bq m^{-2} month^{-1})	Residence Time (d)
0–15°	14.0	7.5
15–30°	12.0	10.7
30–60°	14.8	10.7
60–90°	11.3	19.7

4.2. Seasonal Variation

The monthly values of deposition flux and residence time in the different latitudinal zones are shown in Figure 6. It can be seen that the equatorial zone does not possess strong seasonal variations. In the subtropical zone, its seasonal variation is significant due to its seasonal cycling of semi-arid and semi-humid periods. Deposition is larger in summer and fall and smaller in winter and spring. The average residence time shows a similar trend, except that the seasonal variation is not as evident as that in the deposition flux. This implies that the residence time is not solely determined by the deposition in the zone but by the north–south transport of ^{210}Pb. The mid-latitude zone from 30–60° N also has significant seasonal variations, with deposition reaching the maximum in summer and the minimum in spring. This is similar to the subtropical zone, but with the exception that the decrease in winter relative to summer deposition in the mid-latitude zone is not significant. This suggests that the subtropical and mid-latitude zones may have different reasons for dominating winter deposition. The polar/subpolar regions at 60–90° N show more drastic seasonal variations than the other latitudinal zones. Deposition fluxes are about twice as high in summer as in winter. Atmospheric residence time is significantly longer in winter and spring, around 25 days, with a peak in March. It decreases to only about 10 days in the summer, yet the deposition flux in the summer is almost comparable to or even slightly higher than in the mid-latitude zone. This can be regarded as evidence, implying the significance of northward transport in forming an accumulation zone of ^{210}Pb in the cold months starting from October until the following March or April.

According to Figure 7, it can be seen that the deposition distribution is more concentrated in winter. The distribution is wider in summer than in winter and covers the inland and polar regions where the deposition is much smaller in winter. The reason for this is considered to be the abundance of precipitation in summer compared to the generally low precipitation in winter in the Northern Hemisphere. Although deposition varies significantly between seasons, areas with high (above average) deposition in winter still generally also have significantly high deposition in summer compared to other areas. This may suggest that the areas where high deposition occurs are more or less fixed to geography in the Northern Hemisphere. Deposition on the ocean is significant throughout the year. It also suggests that the distribution of deposition is characterized by the ocean–land distribution. This is consistent with the view provided by observational studies [10]. In addition, it is clear that the Sea of Japan region has ultrahigh deposition in winter than the rest of the Northern Hemisphere. The strong convective weather in the region, which causes much precipitation during winter, is considered to be one of the reasons for this deposition. This will be discussed in detail in Section 4.4.

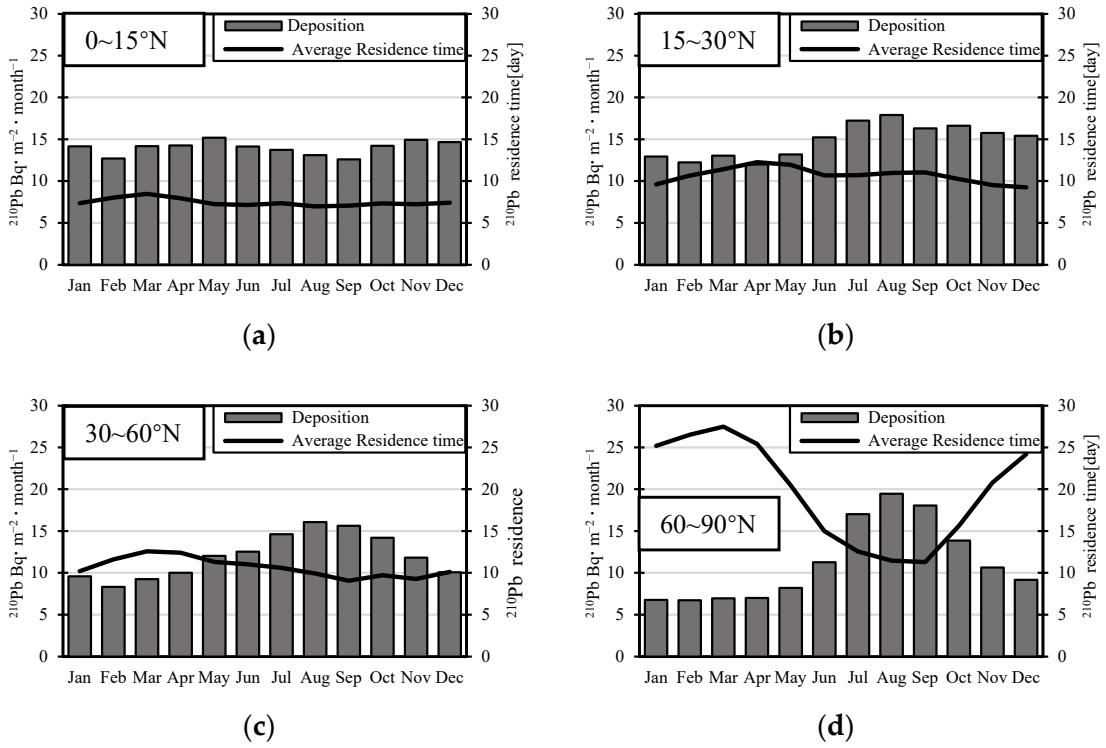

Figure 6. Monthly average of deposition flux and residence time in different latitudinal zones over four years: (**a**) the tropical zone, (**b**) the subtropical zone, (**c**) the mid-latitude zone, (**d**) the polar/subpolar zones.

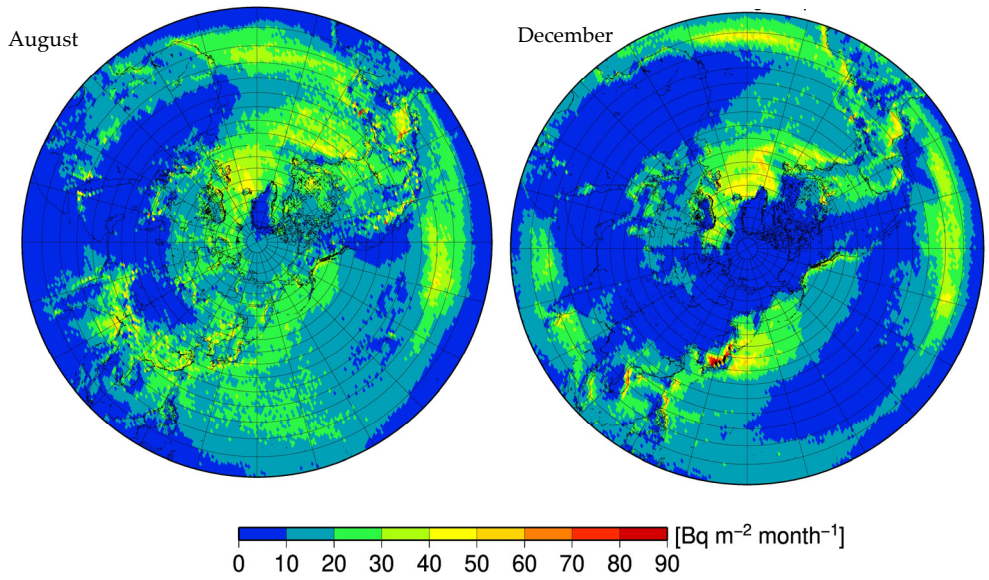

Figure 7. Monthly average of ^{210}Pb depositions in August and December.

The distribution of atmospheric concentrations also shows significant seasonal variations. The distribution of the atmospheric ^{210}Pb concentration integrated into the vertical direction, hereafter referred to as the integral concentration or air-column inventory, is shown in Figure 8 for different seasons. The distribution of atmospheric concentration in winter is higher over continental regions and in polar/subpolar areas, while it is also high in the tropical zone of Western Africa. Summer concentrations are generally higher above 10° N. The drier weather in summer, especially over continental regions, is considered to be the main cause of the clear contrast in the ^{210}Pb concentration distribution between sum-

mer and winter. The low exhalation rate of ^{222}Rn in winter compared to summer [22,24], resulting in low atmospheric ^{210}Pb supplementation, can also be an additional reason.

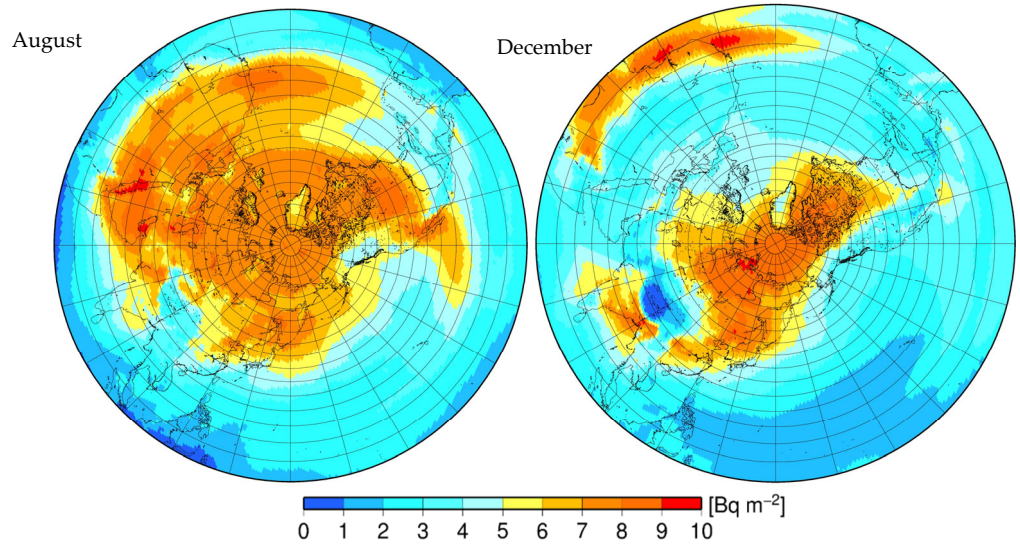

Figure 8. Monthly average of ^{210}Pb atmospheric integral concentrations in August and December.

It was pointed out in Section 4.1 that the seasonal variations in the deposition flux and the residence time are different, depending on the latitudinal zones. The causes of the differences were analyzed as follows. The tropical zone is favorable for the development of tropical depressions because of the high temperatures and humidity throughout the year and the convergence of air currents in the lower atmosphere. This also results in abundant precipitation in the tropical zone [29] and hence, strong deposition. The intertropical convergence zone (ITCZ) is the zone of lowest surface pressure and convergence of air currents between the two subtropical high-pressure belts in the Northern and Southern hemispheres. The ITCZ shifts northward in summer and southward in winter and is located near the equator in spring and fall [30], and the ITCZ enters a strong period from June to August in the Northern Hemisphere, during which it is at its greatest extent, with the southern boundary located near the equator and the northern boundary located near 30° N [31]. This seasonal shift results in a marked increase in precipitation during the subtropical summer and a marked decrease in precipitation during winter, which accompanies the withdrawal of the ITCZ.

Based on the discussion on climatological characteristics of the zones, this seasonal variation in precipitation is considered to be responsible for the increase in deposition in summer and the decrease in winter in the subtropical zone (15–30° N), as shown in Figure 7. The mid-latitude zone (30–60° N) is influenced by the temperate monsoon, and there are significant seasonal changes in precipitation in the continental region. The oceans, on the other hand, have abundant precipitation throughout the year, resulting in slight differences in the winter deposition compared to summer, as shown in Figure 7. Seasonal variability is strongest in the polar/subpolar zones (60–90° N). The longer residence time of ^{210}Pb in winter may be explained by the fact that the Arctic atmosphere ^{210}Pb concentration reaches a maximum in winter [32]. Due to very low precipitation, the removal rate of aerosols carrying ^{210}Pb is low [33]. In contrast, the increase in precipitation during the summer leads to an increase in deposition flux and hence, a lower concentration (Figures 7 and 8) and shorter residence time (Figure 6).

4.3. Vertical Distribution

According to the previous section, the distribution of the atmospheric concentration of ^{210}Pb has a strong influence on deposition and vice versa. In order to investigate

the mechanism, this section discusses the characteristics of the vertical distribution of atmospheric ^{210}Pb concentrations.

The vertical model domain was divided into layers every 3 km: the lower troposphere 0–3 km, the middle troposphere 3–6 km and the upper troposphere 6–9 km layers. The analysis of the ^{210}Pb inventory was conducted for each zone and each month, as shown in Figure 9. The results of the analysis show that the fraction in the lower troposphere was 53% when averaged over the Northern Hemisphere and the four-year period. The fractions of the middle and upper tropospheres were 37% and 10%, respectively. This indicates that at least half of the ^{210}Pb deposition in the Northern Hemisphere is contributed by the lower troposphere and the other half, at the utmost, by the middle and upper tropospheres.

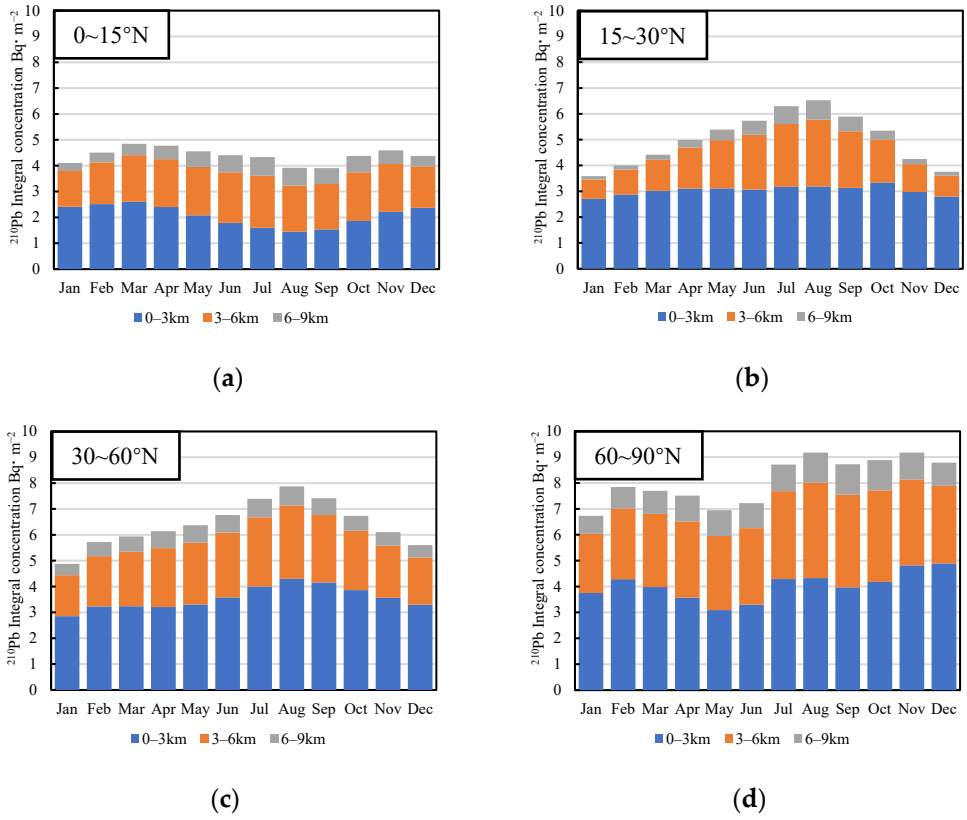

Figure 9. Vertical distribution of atmospheric ^{210}Pb in the different latitudinal zones: (**a**) the tropical zone, (**b**) the subtropical zone, (**c**) the mid-latitude zone, (**d**) the polar/subpolar zones.

The analysis of vertical distribution in different latitude zones shows that in the tropical zone (0–15° N) when the annual average is concerned, the percentage of ^{210}Pb in the middle and upper troposphere is higher (53%) than that in the lower troposphere (47%) (Figure 9). The vertical distribution is less affected by seasons. Enhanced vertical convection due to prolonged sunshine in the zone is considered one of the reasons, as well as the influence of monsoons in the Southern Hemisphere on the zone.

In the subtropical zone (15–30° N), the analysis results show that ^{210}Pb accounts for 61% in the lower troposphere and 39% in the middle and upper tropospheres, as annual averages. The seasonal variation in the ^{210}Pb concentration in the lower troposphere is weak, remaining around 3 Bq m^{-2} throughout the year. The proportion of ^{210}Pb in the middle and upper tropospheres range from 25% in the lowest month of January to 51% in the highest month of August. The proportion of ^{210}Pb in the upper troposphere was 4% in the lowest month of January and 11% in the highest month of August. It can be seen that the vertical distribution of atmospheric ^{210}Pb in the zone has a strong seasonal dependence, and most of its variations come from the seasonal variations in the middle and upper tropospheres. The reason is considered to be that the vertical mixing of ^{210}Pb

in the atmosphere is enhanced by the strong convective weather under the influence of the tropical monsoon in summer, and the parent nuclide of ^{210}Pb, i.e., ^{222}Rn, is vertically mixed and transported to the upper troposphere to perform as a source of ^{210}Pb, resulting in high concentrations in the middle and upper tropospheres. Moreover, extreme climate phenomena such as typhoons are frequent in the zone in summer and can carry more ^{222}Rn from the lower troposphere, where ^{222}Rn is higher than in the layers above to the middle and upper tropospheres, where otherwise its concentration is low. This mechanism, contributed mainly by the middle troposphere as a source of ^{210}Pb, can also lead to more deposition of ^{210}Pb in summer, explaining the strong seasonal variation in deposition in the zone stated in Section 4.1.

In the mid-latitude zone (30–60° N), the middle and upper tropospheres account for 45% of the total atmospheric ^{210}Pb inventory and the lower troposphere for 55%. The vertical distribution is less affected by the seasons when seen from a relative sense, although the total atmospheric inventory varies with the seasons. Deposition in this latitudinal zone is dominated by convective weather, with dry seasons such as summer resulting in high atmospheric concentrations due to reduced precipitation.

The polar/subpolar zones (60–90° N) have a roughly 50/50 ratio between the upper and middle troposphere and the lower troposphere. This ratio does not vary significantly with the seasons. However, atmospheric concentrations in this zone are significantly higher in the second half of the year than in the first half. It is mentioned in Section 4.1 that there is a clear trend of increased deposition in the zone only in summer. It can be reasonably inferred that the enhanced aerosol scavenging prevailing over the polar/subpolar zones during the summer months leads to a high deposition of ^{210}Pb. In turn, atmospheric ^{210}Pb is replenished due to the influx of southern air masses into the region during the summer. Higher concentrations occur in winter, which is considered to correspond with the formation of Arctic haze. The disappearance of these haze layers in the spring is accompanied by a marked decrease in ^{210}Pb concentrations [34].

In order to gain insight into the characterization of the upper atmospheric distribution and its influence on deposition, the distribution of ^{210}Pb concentrations in the 6–9 km height was analyzed. Figure 10 illustrates the horizontal distribution of the integral concentration in this layer of the atmosphere averaged over the four-year period; the horizontal distribution of concentration in the upper troposphere and that of the whole troposphere have similar features. Higher concentrations are found in the subtropical zone and the polar/subpolar zones. The concentration distribution in the mid-latitude zone is significantly lower. Combined with the concentration distribution in Figure 8, it can be said that most of the concentration in the mid-latitude zone is distributed in the middle and lower tropospheres. Comparing the distributions in winter and summer in Figure 10, it is evident that there is a significant overall increase in the concentration in the upper troposphere in summer compared to that in winter. This can be attributed to stronger vertical mixing of the atmosphere in summer. The areas of higher concentrations in summer are in the arid subtropics and the polar/subpolar zones. In winter, the concentrations in the subtropics are significantly lower, and the concentrations in the polar/subpolar zones are slightly lower but still high compared to the other zones. Combined with the seasonal variations in the distribution of deposition in the subtropical zone, it is highly probable that the concentration in the upper troposphere contributes to deposition in the subtropical zone in summer. The high concentrations in the polar/subpolar zones in winter are likewise considered to be related to the build-up of the Arctic haze mentioned earlier.

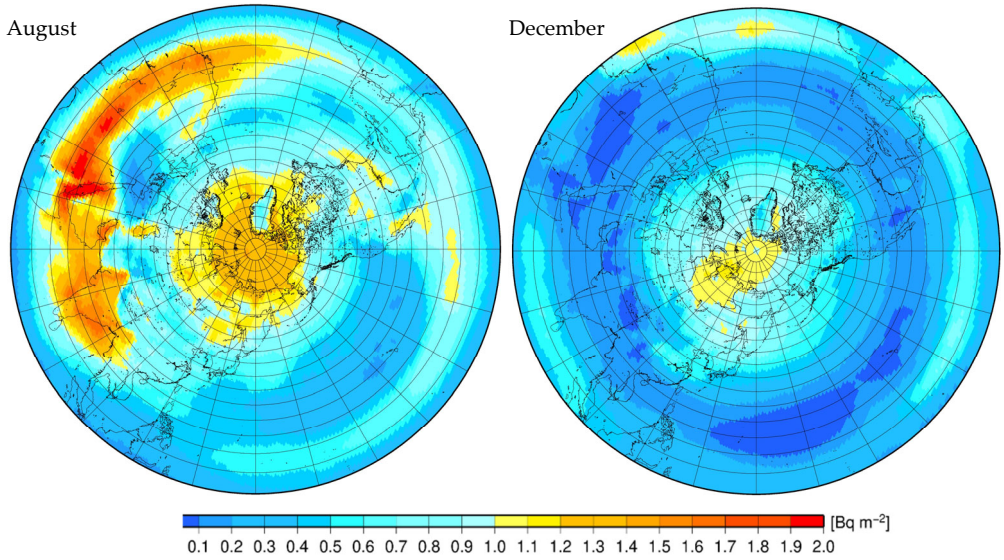

Figure 10. Concentration distribution of four-year average integral concentration of ^{210}Pb in the upper troposphere (6–9 km).

4.4. Horizontal Distribution in the Far East Region

The Sea of Japan region is known to have a high deposition based on previous studies. As can be seen in Figure 7, especially during the winter months, the Sea of Japan region is characterized by an enormous ^{210}Pb deposition if compared with other regions over the Northern Hemisphere. Also, according to the results mentioned above, the Sea of Japan region is the typical region in the Northern Hemisphere that produces large spatial differences in deposition distribution at the exit of continental air masses. The four-year average horizontal deposition distribution in this region is shown in Figure 11a. It can be seen that deposition in the coastal region of the Sea of Japan is 5–6 times higher than in the upwind continental region, i.e., eastern China and Siberia. Figure 11b shows that the horizontal distribution of concentrations is opposite to that of deposition, with significantly higher concentrations in the upwind continent than in the Sea of Japan region. The horizontal distribution of residence time in the atmosphere, shown in Figure 11c, illustrates that the average residence time in the upwind continent is in the range of 20–80 days, which is significantly longer than that in the downwind region around Japan in the range of 3–15 days. It is reasonable to assume that the high concentration of ^{210}Pb (region is at the white dashed box in Figure 11.) travels downwind to the Sea of Japan region (direction by the black arrow in Figure 11.)with the movement of air masses caused by the winter monsoon, and then deposition occurs along with precipitation. The winter monsoon is originally cold and dry until it comes to the Sea of Japan, causing less deposition over the continent, and accumulation of ^{210}Pb occurs in the air, as shown in Figure 11. Once reaching the Sea of Japan, the air mass gains heat and moisture from the sea surface affected by the Tsushima warm current, causing much precipitation along the Sea of Japan side of the Japanese Islands and hence, much deposition there. Although the coarse horizontal grid of the present study failed to depict the very sharp contrast in deposition and precipitation distributions, these characteristics were, to some extent, reproduced.

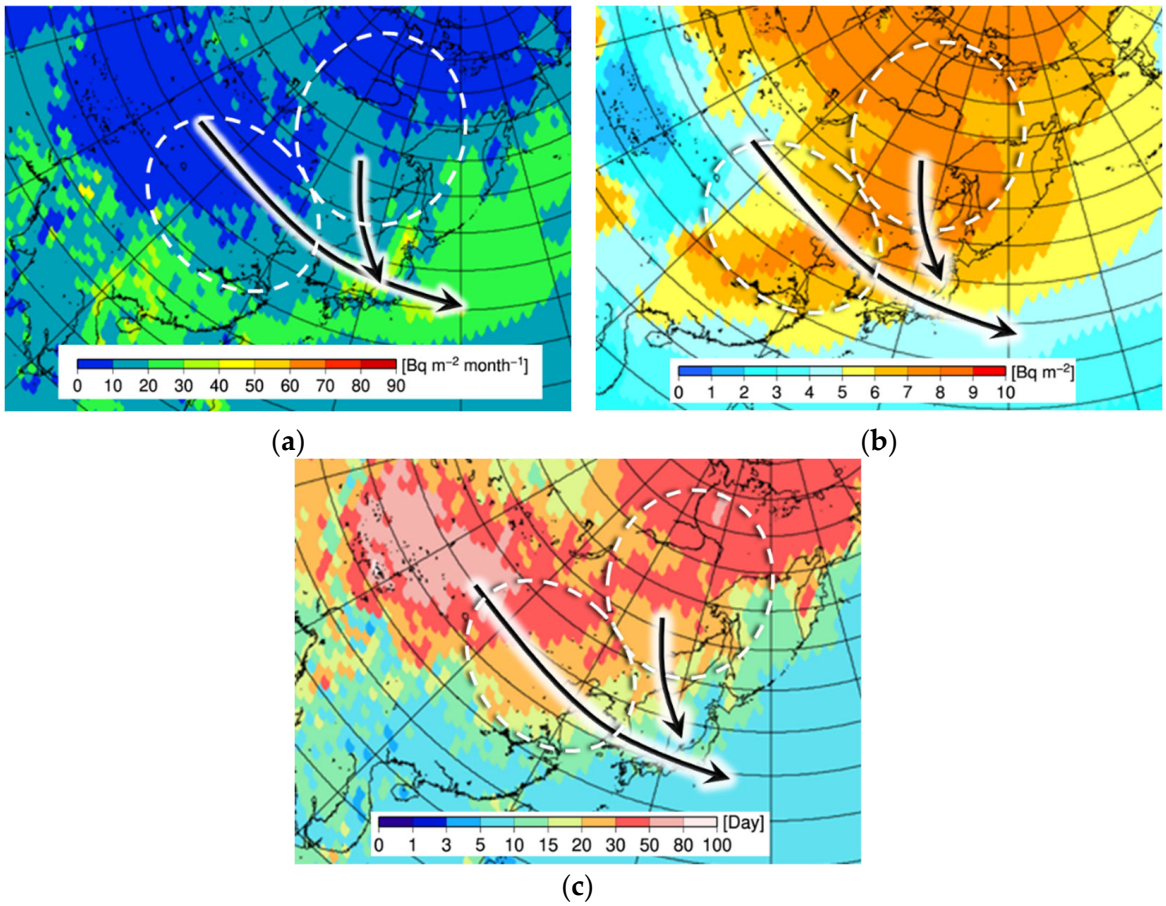

Figure 11. Four-year (2012–2015) monthly average of (**a**) ^{210}Pb deposition flux, (**b**) integral ^{210}Pb concentration, and (**c**) ^{210}Pb residence time in the atmosphere.

To verify this phenomenon, we analyzed the deposition flux and the atmospheric residence time of ^{210}Pb in the upwind and downwind areas, as shown in Figure 12. It can be seen that the deposition flux in the two upwind regions and the Sea of Japan region show a significant negative correlation. The average residence time shows that the months with a long residence time in the upwind (e.g., December) have significantly shorter residence times in the downwind. It is reasonable to assume that when deposition in the upwind region consumes most of the atmospheric ^{210}Pb, the inventory of the atmospheric ^{210}Pb that is available for deposition in the downwind region depletes, leading to a reduced deposition in the downwind region. Therefore, it can be said that the source of ^{210}Pb deposited in the Sea of Japan region is the ^{210}Pb in the atmosphere in the upwind continental region. Since the deposition distribution is reported to be strongly correlated with precipitation [4], it can be concluded that the high deposition distribution around Japan is particularly influenced by the monsoon, which causes much precipitation during winter along the Sea of Japan coastlines of the Japanese Islands.

Based on the above discussions, the high depositions in the Northwestern Pacific and North Atlantic Ocean regions found in Figure 3 are considered to have the same mechanism as that in the Japanese region. The high deposition regions over the oceans are considered to be caused by precipitation accompanying the migration of low-pressure systems in these regions. The low-pressure systems draw in continental air that is abundant with ^{210}Pb built up over the continental area and deposit it on the ocean surfaces by precipitation.

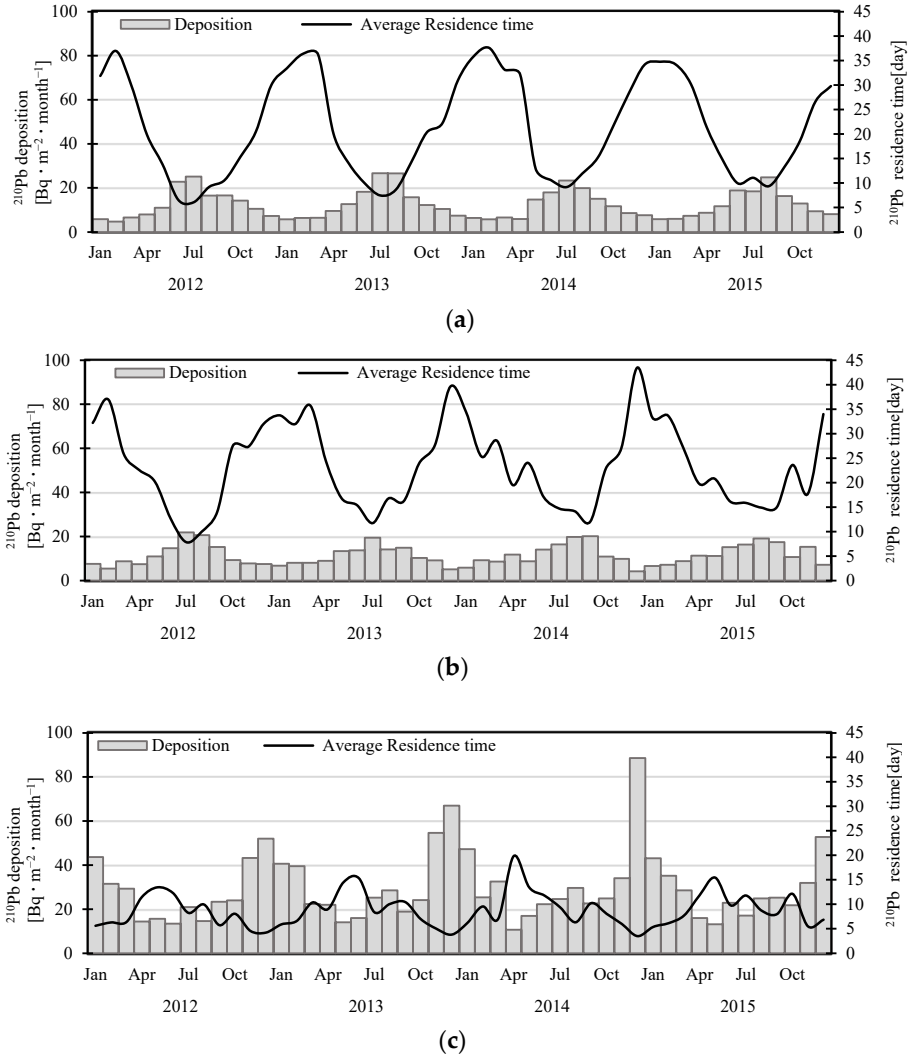

Figure 12. ^{210}Pb deposition flux and residence time in 2012–2015: (**a**) average values for the Siberian region (40°–60° N, 110°–140° E); (**b**) eastern China region (30°–40° N, 100°–120° E) and (**c**) Sea of Japan coastal region for which averages of the following four regions were taken (35°–38° N, 132–135° E), (35°–39° N, 135°–138° E), (36°–41° N, 138°–140° E) and (41°–43° N 138°–142° E).

5. Conclusions

In this study, we used the atmospheric transport model consisting of WRF and HIRAT to calculate the transportation and deposition of ^{210}Pb in the Northern Hemisphere over the four-year period 2012–2015. A comparison of model calculations with observations showed that the calculated annual deposition fluxes at most of the observation sites were generally in reasonable agreement with the observed values.

The calculation results showed that the four-year average deposition flux in the Northern Hemisphere was 13.0 Bq m^{-2} month^{-1}, and the deposition distribution had strong seasonal variations. The depositional flux was generally higher in summer and lower in winter. The deposition distribution in the Northern Hemisphere had a clear dependence on the sea–land distribution. Furthermore, the average atmospheric residence time of ^{210}Pb in regions with a high deposition was estimated to be in the range of 3–10 days, while that in regions with a low deposition can be as long as 30 days.

In addition, deposition was found to have different patterns and mechanisms in different latitudinal zones. Deposition is highest in the tropical zone and lowest in the polar/subpolar zones. There is also a latitudinal dependence on atmospheric residence time. Additionally, there is a strong seasonal dependence of ^{210}Pb deposition and transport

characteristics in different latitudinal zones. Seasonal variations are the smallest in the equatorial zone and most pronounced in the polar/subpolar zones.

The results also indicate that there is also a seasonal dependence of atmospheric ^{210}Pb concentration variations. In summer, the distribution of high atmospheric ^{210}Pb concentrations is wider in its horizontal extent due to dry weather, and in winter, the distribution of high atmospheric concentrations is smaller due to more humid weather than in summer. It is noteworthy that the polar/subpolar regions have high atmospheric concentrations throughout the year.

Analysis of the vertical distribution of atmospheric ^{210}Pb shows that the lower troposphere (0–3 km) dominates with a share of about 53%. The middle troposphere (3–6 km) accounts for 37%, and the upper troposphere (6–9 km) for about 10%. This distribution did not significantly change seasonally in the equatorial and polar/subpolar zones; however, in the subtropical and mid-latitude zones, the proportion of the total ^{210}Pb in the upper and middle tropospheres is significantly larger in summer than in winter. In winter, it was as low as about 25%. This result suggests the possibility that the middle and upper tropospheres also contribute to horizontal transport and hence, the deposition of ^{210}Pb.

The mechanisms that dominate deposition were also analyzed in this study. The Japan Sea region, which has the most significant deposition in the Northern Hemisphere in the calculation results, was focused on as the object of analysis. It was clearly demonstrated that the mid to eastern part of the Eurasian continent, where depletion of atmospheric ^{210}Pb inventory due to deposition was weak during winter, worked as an area of building up ^{210}Pb-rich air masses that outflowed over to Japan and the Northwestern Pacific Ocean by the winter monsoon to cause heavy deposition onto the land and ocean surfaces via precipitation accompanying the low-pressure systems. This monsoon-low-pressure regime is considered to be the main factor for determining the distribution of ^{210}Pb deposition.

Author Contributions: Conceptualization, H.Y. and Y.C.; methodology, H.Y.; software, Y.C.; validation, Y.C., H.Y. and T.I.; formal analysis, Y.C.; investigation, Y.C.; resources, H.Y. and T.I.; data curation, Y.C.; writing—original draft preparation, Y.C.; writing—review and editing, H.Y. and T.I.; visualization, Y.C.; supervision, H.Y. and T.I.; project administration, H.Y. and T.I.; funding acquisition, H.Y. All authors have read and agreed to the published version of the manuscript.

Funding: This research was funded by JSPS KAKENHI, grant number 20H04321. And ERAN, grant number Y-23-11.

Institutional Review Board Statement: Not applicable.

Data Availability Statement: Not applicable.

Conflicts of Interest: The authors declare no conflict of interest.

Appendix A

Table A1. Variable definition.

Variable Name	Variable Definition
h	Depth of model domain (m)
I	Precipitation intensity (mm h^{-1})
K_{z^*}	Vertical diffusion coefficient (m^2 s^{-1})
m	Map factor
Q	Atmospheric concentration (Bq m^{-3})
u	Wind speed in x direction (m s^{-1})
v	Wind speed in y direction (m s^{-1})
v_d	Deposition velocity (m s^{-1})
w^*	Wind speed in the vertical direction (m s^{-1})
z	Vertical coordinates of the Cartesian coordinate system (m)
z_g	Ground surface altitude (elevation) above sea level (m)
z_t	Altitude at the top of the calculation domain (m)
Λ	Scavenging coefficient (s^{-1})
λ	Decay constant (s^{-1})

References

1. United Nations Scientific Committee on the Effects of Atomic Radiation. *Sources and Effects of Ionizing Radiation: UNSCEAR 2008 Report to the General Assembly, with Scientific Annexes*; United Nations: New York, NY, USA, 2010; ISBN 978-92-1-142274-0.
2. Nuclear Safety Research Association. *Seikatsu-Kankyo-Houshsen (Radiation in Living Environment)*, 3rd ed.; Nuclear Safety Research Association: Tokyo, Japan, 2020. (In Japanese)
3. Hirose, K.; Kikawada, Y.; Doi, T.; Su, C.-C.; Yamamoto, M. ^{210}Pb Deposition in the Far East Asia: Controlling Factors of Its Spatial and Temporal Variations. *J. Environ. Radioact.* **2011**, *102*, 514–519. [CrossRef] [PubMed]
4. Yamamoto, M.; Sakaguchi, A.; Sasaki, K.; Hirose, K.; Igarashi, Y.; Kim, C.K. Seasonal and Spatial Variation of Atmospheric ^{210}Pb and 7Be Deposition: Features of the Japan Sea Side of Japan. *J. Environ. Radioact.* **2006**, *86*, 110–131. [CrossRef] [PubMed]
5. Baskaran, M. Po-210 and Pb-210 as Atmospheric Tracers and Global Atmospheric Pb-210 Fallout: A Review. *J. Environ. Radioact.* **2011**, *102*, 500–513. [CrossRef] [PubMed]
6. Alonso-Hernández, C.M.; Morera-Gómez, Y.; Cartas-Águila, H.; Guillén-Arruebarrena, A. Atmospheric Deposition Patterns of ^{210}Pb and ^{7}Be in Cienfuegos, Cuba. *J. Environ. Radioact.* **2014**, *138*, 149–155. [CrossRef]
7. Magnoni, M.; Bellina, L.; Bertino, S.; Bellotto, B.; Chiaberto, E. Evaluation of the Terrestrial 222Rn Flux from ^{210}Pb Deposition Measurements. *Environments* **2022**, *9*, 68. [CrossRef]
8. Leppänen, A.-P. Deposition of Naturally Occurring 7Be and 210Pb in Northern Finland. J. Environ. Radioact. 2019, 208–209, 105995. *J. Environ. Radioact.* **2019**, *208–209*, 105995. [CrossRef]
9. Peng, A.; Liu, G.; Jiang, Z.; Liu, G.; Liu, M. Wet Depositional Fluxes of ^{7}Be and ^{210}Pb and Their Influencing Factors at Two Characteristic Cities of China. *Appl. Radiat. Isot.* **2019**, *147*, 21–30. [CrossRef]
10. Lozano, R.L.; San Miguel, E.G.; Bolívar, J.P.; Baskaran, M. Depositional Fluxes and Concentrations of ^{7} Be and ^{210} Pb in Bulk Precipitation and Aerosols at the Interface of Atlantic and Mediterranean Coasts in Spain. *J. Geophys. Res.* **2011**, *116*, D18213. [CrossRef]
11. Baskaran, M.; Shaw, G.E. Residence Time of Arctic Haze Aerosols Using the Concentrations and Activity Ratios of ^{210}Po, ^{210}Pb and ^{7}Be. *J. Aerosol Sci.* **2001**, *32*, 443–452. [CrossRef]
12. Cai, Y.; Yamazawa, H.; Moriizumi, J.; Hasegawa, H. Analysis of ^{210}PB Deposition Distribution Characteristics in Winter at Rokkasho in Aomori Based on High Resolution Atmospheric Transport/Deposition Model Calculation. *Radiat. Prot. Dosim.* **2022**, *198*, 914–919. [CrossRef]
13. Yamazawa, H.; Cai, Y.; Matsumoto, T.; Moriizumi, J.; Hasegawa, H.; Kawano, T. Long-Range Atmospheric Transport of Radon in East Asia and Deposition of Its Progenies In Japan. *Radiat. Prot. Dosim.* **2022**, *198*, 891–895. [CrossRef] [PubMed]
14. Hirao, S.; Yamazawa, H.; Moriizumi, J.; Yoshioka, K.; Iida, T. Development and Verification of Long-Range Atmospheric Radon-222 Transport Model. *J. Nucl. Sci. Technol.* **2008**, *45*, 166–172. [CrossRef]
15. Ueno, T.; Nagao, S.; Yamazawa, H. Atmospheric Deposition of ^{7}Be, 40K, 137Cs and ^{210}Pb during 1993–2001 at Tokai-Mura, Japan. *J. Radioanal. Nucl. Chem.* **2003**, *255*, 335–339. [CrossRef]
16. Skamarock, W.C.; Klemp, J.B.; Dudhia, J.; Gill, D.O.; Barker, D.M.; Duda, M.G.; Huang, X.-Y.; Wang, W.; Powers, J.G. *A Description of the Advanced Research WRF Version 3*; National Center for Atmospheric Research: Boulder, CO, USA, 2008.
17. Hong, S.-Y.; Dudhia, J.; Chen, S.-H. A Revised Approach to Ice Microphysical Processes for the Bulk Parameterization of Clouds and Precipitation. *Mon. Weather Rev.* **2004**, *132*, 103–120. [CrossRef]
18. Chen, F.; Dudhia, J. Coupling an Advanced Land Surface–Hydrology Model with the Penn State–NCAR MM5 Modeling System. Part I: Model Implementation and Sensitivity. *Mon. Weather Rev.* **2001**, *129*, 569–585. [CrossRef]
19. Nakanishi, M.; Niino, H. An Improved Mellor–Yamada Level-3 Model: Its Numerical Stability and Application to a Regional Prediction of Advection Fog. *Bound.-Layer Meteorol.* **2006**, *119*, 397–407. [CrossRef]
20. Arakawa, A. Computational Design of the Basic Dynamical Processes of the UCLA General Circulation Model. *Gen. Circ. Models Atmos.* **1977**, *17*, 173–265.
21. Yamazawa, H. Development of a Numerical Solution Method for Advection Terms and Its Application to the Atmospheric Dynamic Model, PHYSIC. *J. Nucl. Sci. Technol.* **1996**, *33*, 69–77. [CrossRef]
22. Crank, J.; Nicotson, E. *A Practical Method for Numerical Evaluation of Solutions of Partial Differential Equations of the Heat-Conduction Type*; Cambridge University Press: Cambridge, UK, 1947.
23. Schery, S.D.; Wasiolek, M.; Nemetz, B.M.; Yarger, F.D.; Whittlestone, S. Modeling Radon Flux from the Earth's Surface. *Aerosol Sci. Technol.* **1998**, *28*, 207–217.
24. Yamazawa, H.; Hirao, S.; Moriizumi, J.; Iida, T. Evaluation of Radon Flux Maps for Siberian and East Asian Regions by Using Atmospheric Radon Concentration Observed Over Oceans. In Proceedings of the EA/WMO Technical Meeting, Vienna, Austria, 22–24 June 2009.
25. Hirao, S.; Yamazawa, H.; Moriizumi, J. Inverse Modeling of Asian ^{222}Rn Flux Using Surface Air ^{222}Rn Concentration. *J. Environ. Radioact.* **2010**, *101*, 974–984. [CrossRef]
26. Wang, Z.; Yang, W.; Chen, M.; Lin, P.; Qiu, Y. Intra-Annual Deposition of Atmospheric ^{210}Pb,^{210}Po and the Residence Times of Aerosol in Xiamen, China. *Aerosol Air Qual. Res.* **2014**, *14*, 1402–1410. [CrossRef]
27. Winkler, R.; Rosner, G. Seasonal and Long-Term Variation of ^{210}Pb Concentration in Air, Atmospheric Deposition Rate and Total Deposition Velocity in South Germany. *Sci. Total Environ.* **2000**, *263*, 57–68. [CrossRef] [PubMed]

28. Ali, N.; Khan, E.U.; Akhter, P.; Rana, M.A.; Rajput, M.U.; Khattak, N.U.; Malik, F.; Hussain, S. Wet Depositional Fluxes of ^{210}Pb and ^{7}Be-Bearing Aerosols at Two Different Altitude Cities of North Pakistan. *Atmos. Environ.* **2011**, *45*, 5699–5709. [CrossRef]
29. Lashkari, H.; Jafari, M. Annual Displacement and Appropriate Index to Determine ITCZ Position in East Africa and the Indian Ocean Regions. *Meteorol. Atmos. Phys.* **2021**, *133*, 1111–1126. [CrossRef]
30. Kang, S.M.; Shin, Y.; Xie, S.-P. Extratropical Forcing and Tropical Rainfall Distribution: Energetics Framework and Ocean Ekman Advection. *npj Clim. Atmos. Sci.* **2018**, *1*, 20172. [CrossRef]
31. Yang, T. Seasonal and Interannual Variation Characteristics of the Tropical Indian Ocean's Intertropical Convergence Zone. *Clim. Change Res. Lett.* **2021**, *10*, 584–597. [CrossRef]
32. Dibb, J.E.; Meeker, L.D.; Finkel, R.C.; Southon, J.R.; Caffee, M.W.; Barrie, L.A. Estimation of Stratospheric Input to the Arctic Troposphere: ^{7} Be and ^{10} Be in Aerosols at Alert, Canada. *J. Geophys. Res.* **1994**, *99*, 12855. [CrossRef]
33. Shaw, G.E. Aerosol Chemical Components in Alaska Air Masses: 1. *Aged Pollution. J. Geophys. Res.* **1991**, *96*, 22357. [CrossRef]
34. Feely, H.W.; Larsen, R.J.; Sanderson, C.G. Factors That Cause Seasonal Variations in Beryllium-7 Concentrations in Surface Air. *J. Environ. Radioact.* **1989**, *9*, 223–249. [CrossRef]